Observation of Floquet States in a Strongly Driven Artificial Atom

Chunqing Deng,[1,*] Jean-Luc Orgiazzi,[2] Feiruo Shen,[1] Sahel Ashhab,[3] and Adrian Lupascu[1]
[1]Institute for Quantum Computing, Department of Physics and Astronomy, and Waterloo Institute for Nanotechnology, University of Waterloo, Waterloo, Ontario, Canada N2L 3G1
[2]Institute for Quantum Computing, Department of Electrical and Computer Engineering, and Waterloo Institute for Nanotechnology, University of Waterloo, Waterloo, Ontario, Canada N2L 3G1
[3]Qatar Environment and Energy Research Institute (QEERI), HBKU, Qatar Foundation, Doha, Qatar
(Received 21 May 2015; published 24 September 2015)

We present experiments on the driven dynamics of a two-level superconducting artificial atom. The driving strength reaches 4.78 GHz, significantly exceeding the transition frequency of 2.288 GHz. The observed dynamics is described in terms of quasienergies and quasienergy states, in agreement with Floquet theory. In addition, we observe the role of pulse shaping in the dynamics, as determined by nonadiabatic transitions between Floquet states, and we implement subnanosecond single-qubit operations. These results pave the way to quantum control using strong driving with applications in quantum technologies.

DOI: 10.1103/PhysRevLett.115.133601 PACS numbers: 42.50.Ct, 42.50.Dv, 42.50.Hz, 85.25.Cp

Monochromatic driving is the most common tool in quantum control, applicable to various physical systems including nuclear and electronic spins, atoms, ions, superconducting qubits, and quantum dots [1]. For driving that is weak compared to the relevant transition frequency, the dynamics can be described in terms of Rabi oscillations between energy eigenstates. In contrast, with strong driving the commonly used rotating wave approximation [2] breaks down, resulting in complex evolution. Strong driving dynamics is most adequately described in the framework of Floquet theory [3], where the state of a driven system is expressed in terms of quasienergies and quasienergy states. Exploring this more general framework expands the field of quantum control, gaining increasing relevance as current experiments on the implementation of high-fidelity quantum gates [4] and protection against decoherence [5] are performed with a driving strength that is a significant fraction of the transition frequency. In addition, strong driving is relevant in the fields of quantum sensing, for phase measurements [6], and quantum simulation, for designing effective Hamiltonians in the emerging field of Floquet engineering [7].

In this Letter we report experiments on the dynamics of an artificial atom, a superconducting quantum bit [8,9], strongly driven by a microwave field. Strong driving has been studied in the field of atomic physics, using either optical [10] or radio frequency pulses [6]. In experiments with NV centers in diamond, time dynamics was observed for driving strength up to values comparable to the transition frequency [11]. Superconducting qubits display a naturally strong coupling to electromagnetic fields due to their mesoscopic character. Previous experiments on strong driving of superconducting qubits have mostly addressed the steady-state response to continuous waves [12–22]. A few experiments have observed time-domain Rabi oscillations [23–25] with a driving strength exceeding the transition frequency, and two of these demonstrated good agreement with the theoretically predicted Bessel-function dependence of the Rabi frequency [23,25]. In our experiments, we use quantum state tomography to investigate the dynamics of a superconducting qubit strongly driven by microwave pulses with controllable shape. The observed system dynamics is very well described in terms of quasienergies and quasienergy states, as predicted by Floquet theory. In particular, we observe several frequency components in the dynamics, in very good agreement with theory. We find that the switching on and off of the driving pulse plays an important role in the qubit evolution, as determined by adiabaticity conditions in the Floquet picture [26]. We also used strong driving for fast, subnanosecond, preparation of qubit states.

The artificial atom in our experiment is a superconducting flux qubit [27]. Among the different types of superconducting qubits, flux qubits have the advantage of high-level anharmonicity, leading to ideal two-level system behavior, and of strong coupling to electromagnetic fields [28,29], which enable strong driving. Qubit state measurement is performed by probing microwave transmission through a resonator coupled to the qubit [see Fig. 1(a)], in the dispersive regime of circuit quantum electrodynamics [30].

The qubit Hamiltonian is given by $H(t) = -(\hbar\Delta/2)\sigma_z - [\hbar\epsilon(t)/2]\sigma_x$ in a basis formed by symmetric and antisymmetric combinations of clockwise and anticlockwise persistent current states in the qubit loop [27]. Here Δ, the minimum energy level splitting, is a fixed parameter, and $\epsilon(t) = 2I_p(\Phi(t) - \Phi_0/2)$, with $\Phi(t)$ the magnetic flux applied to the loop dependent on the time t. The magnetic

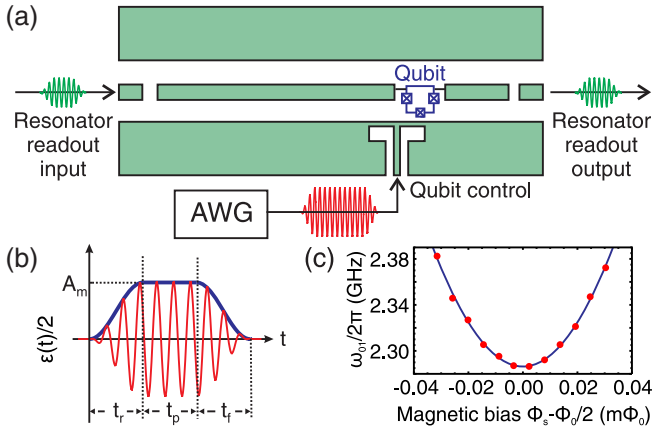

FIG. 1 (color online). (a) Schematic representation of the experimental setup. The qubit, formed by a superconducting loop interrupted by Josephson junctions (cross symbols), is coupled to a superconducting coplanar waveguide resonator. Readout is based on the transmission of a microwave pulse from the resonator input (left) to its output port (right). A waveguide (bottom) is used to couple microwave control pulses to the qubit. (b) Representation of qubit control pulses, with rise and fall times t_r and t_f, respectively, and maximum-amplitude duration t_p. The thick line indicates the pulse envelope, which reaches a maximum A_m. During rise and fall, the envelope is shaped as $(A_m/2)[1-\cos(\pi t/t_r)]$ and $(A_m/2)\{1+\cos[\pi(t-t_p-t_r)/t_f]\}$. (c) Qubit transition frequency ω_{01} from spectroscopy measurements versus the static magnetic flux Φ_s. The continuous line is a fit of the transition frequency, yielding the parameters $\Delta = 2\pi \times 2.288$ GHz and $I_p = 690$ nA.

flux $\Phi(t) = \Phi_s + \Phi_d(t)$, with Φ_s a static flux generated by a superconducting coil and $\Phi_d(t)$ a time-varying magnetic flux coupled to the qubit through a waveguide terminated by an antenna [see Fig. 1(a)]. The usual approach employed to generate control pulses is based on using a modulator to shape the quadratures of a continuous wave produced by a frequency synthesizer. Here we use instead a new generation of high-speed arbitrary waveform generator (AWG) to directly synthesize the microwave pulses [31], leading to the time accuracy required for control with subnanosecond resolution pulses.

A plot of the qubit transition frequency versus the static flux Φ_s, obtained by spectroscopy with weak and long microwave pulses, is shown in Fig. 1(c). All the experiments reported in this Letter are performed at the symmetry point ($\Phi_s = \Phi_0/2$), where the qubit transition frequency $\omega_{01} = \Delta = 2\pi \times 2.288$ GHz. We use amplitude shaped pulses $\epsilon(t) = 2A(t)\cos(\omega t)$, with $A(t)$ characterized by a maximum amplitude A_m and rise and fall times denoted by t_r and t_f, respectively [see Fig. 1(b)]. At the symmetry point, the energy relaxation and pure dephasing times are given by $T_1 = 1.8$ μs and $T_{\text{Ramsey}} = 0.3$ μs. These coherence times, currently limited by quasiparticle tunneling, microscopic two-level systems, and charge noise [36,37], can be further improved by infrared shielding techniques and improved qubit design without impairing the ability to strongly drive the qubit.

Experiments are performed by repeating, typically 16,384 times, a sequence formed of state reset, control using an applied pulse, and measurement in the energy eigenbasis. Figure 2(a) shows the qubit's average excited state probability versus the duration of the microwave pulse, with driving on resonance. The waveform is defined with zero rise or fall times; however, the actual rise and fall times are determined by the analog bandwidth of the AWG and are specified to be shorter than 22 ps [31]. For weak driving [Fig. 2(a), top panel], sinusoidal oscillations are obtained, as predicted based on the rotating wave approximation. With a large Rabi driving strength [Fig. 2(a), bottom panel], large amplitude oscillations are accompanied by smaller amplitude faster oscillations, a signature of non-negligible counterrotating term effects. The different frequency components are clearly visible in the Fourier transform of the signal [Fig. 2(b)]. For a wide range of the driving strength A_m, from $2\pi \times 0.20$ GHz to $2\pi \times 4.78$ GHz, the Fourier transformed data are shown in Fig. 2(c).

The presence of the various frequency components in the Rabi oscillations can be understood based on Floquet theory, which predicts that for a time-periodic Hamiltonian with period T the quantum state is given by $|\psi(t)\rangle = \sum_{j=0,1} c_j e^{-i\epsilon_j t}|u_j(t)\rangle$, with ϵ_j the quasienergies and $|u_j(t)\rangle$ the quasienergy states, periodic in time with period T. As a result, the probability to find the system in its excited state is expected to show oscillatory behavior with frequency components $n\omega$ and $\pm\Delta\epsilon + n\omega$, with $\Delta\epsilon$ the quasienergy difference, $\omega = 2\pi/T$ the driving frequency, and n any integer number. The harmonic drive signal used in our experiment has the additional symmetry $\epsilon(t + T/2) = -\epsilon(t)$, and as a result only components with even n values are present [38]. Figure 2(d) shows the extracted frequency components versus driving amplitude. We compare the experimental results with calculations of the quasienergies based on numerical simulations (solid lines) and an analytical expression (dashed lines). The latter, obtained based on approximate diagonalization after transformation to a rotating frame [31], gives a quasienergy difference $\Delta\epsilon = \omega\sqrt{[1 - J_0(2A/\omega)]^2 + J_1^2(2A/\omega)}$, with J_0 or J_1 the Bessel function of the first kind and order 0 or 1. This formula provides a good approximation for the case of a two-level system biased at its symmetry point and driven on or near resonance with arbitrary strength, complementing previous theoretical work where the weak- and strong-driving limits of this formula had been derived [21,22]. Additional experiments were performed with the qubit driven off resonance, with a driving frequency $\omega = 2\pi \times 1.373$ GHz [see Figs. 2(e) and 2(f)]. The Fourier transform of the qubit population signal and the identified frequency components are shown in Figs. 2(g) and 2(h), respectively. Good agreement with the predictions of

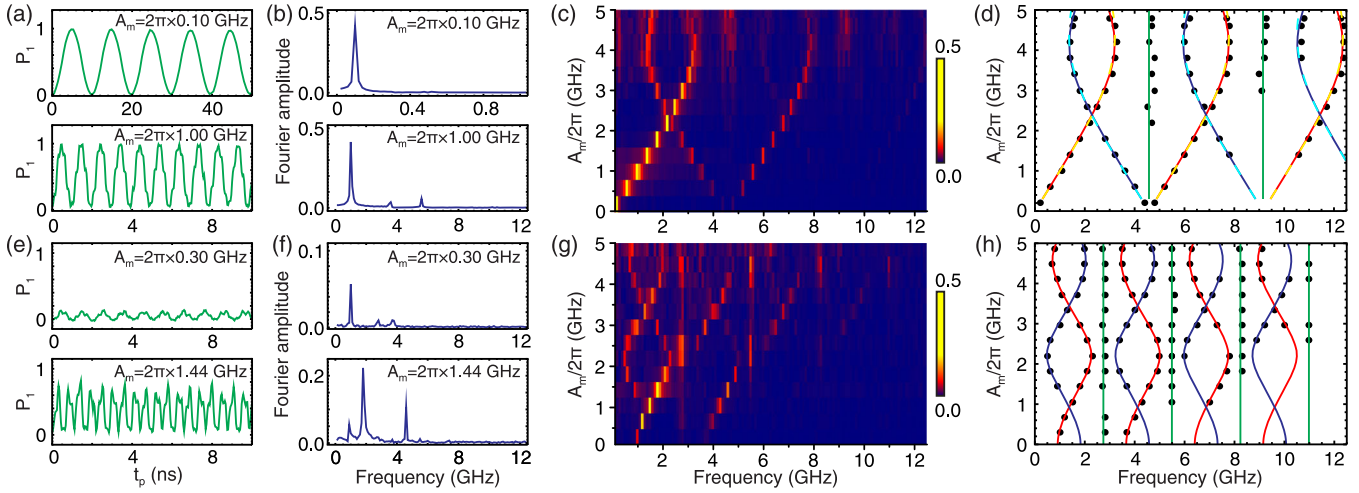

FIG. 2 (color online). Coherent oscillations versus driving amplitude for (a)–(d) resonant driving ($\omega = \Delta$) and (e)–(h) off-resonance driving ($\omega = 0.6\Delta$). (a),(e) Qubit excited state probability P_1 versus control pulse duration t_p for (a) $A_m = 0.10$ and 1.00 GHz and (e) $A_m = 0.30$ and 1.44 GHz. (b),(f) Discrete Fourier transforms of the oscillations in (a) and (e), respectively. (c),(g) Color plot of the Fourier transform of population oscillations versus frequency and driving pulse amplitude. (d),(h) Positions of peaks in the Fourier transform of coherent oscillations versus driving amplitude extracted from the data in (c) and (g) (dots). The lines are plots of $n\omega$, $n\omega - \Delta\epsilon$, and $n\omega + \Delta\epsilon$, respectively, with the quasienergy difference $\Delta\epsilon$ determined numerically and n an even integer. For the resonant driving case (d), we show in addition corresponding curves (dashed) based on the analytical approximation for $\Delta\epsilon$ discussed in the text (see also Ref. [31]).

numerical calculations is observed in this case as well [see Fig. 2(h)].

Tomography experiments confirm the role of the counter-rotating terms in the driven evolution of the qubit. Figure 3 shows results of state tomography versus the duration of driving pulses for two values of the driving amplitude,

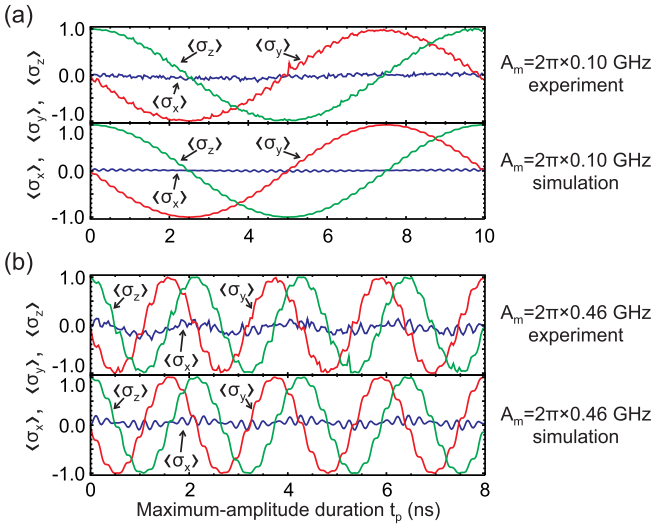

FIG. 3 (color online). Measurements and simulations of the evolution of the Bloch vector components, given by the average values of the Pauli σ_α ($\alpha = x, y, x$) operators, after a pulse with zero rise and fall time, versus the length of the pulse for (a) $A_m = 2\pi \times 0.10$ GHz and (b) $A_m = 2\pi \times 0.46$ GHz. The experimental results are in excellent agreement with the results of numerical simulations.

$A_m = 2\pi \times 0.10$ GHz and $A_m = 2\pi \times 0.46$ GHz, and zero rise and fall times. For both values of the driving amplitude, high-amplitude oscillations are observed, with a period corresponding to the quasienergy difference. In the weak-driving limit, these oscillations are the usual Rabi oscillations. High-frequency components are observed in addition, with a significant amplitude at strong driving, reflecting the presence of the non-negligible counterrotating wave component. The results of tomography experiments are in very good agreement with predictions of numerical simulations of the Schrödinger equation (see Fig. 3).

The presence of the fast oscillatory terms in the driven evolution depends not only on the pulse amplitude but also on the pulse turn-on and turn-off times. Figure 4(a) shows qubit state oscillations for a driving strength $A_m = 2\pi \times 1.33$ GHz, and different rise and fall times. Fast oscillatory terms are gradually suppressed as the turn-on and turn-off times are increased. We emphasize that fast oscillatory components in the oscillations are completely suppressed for slow pulse turn-on and turn-off despite the fact that during most of the driven evolution the driving amplitude is comparable with the transition frequency. The absence of fast oscillations for slow turn-on and turn-off can be understood based on adiabaticity in the Floquet picture [26]. Indeed, the time-dependent qubit state can be written, up to an overall phase and a geometric phase, as $|\psi(t)\rangle = c_0(t)|u_0(A,t)\rangle + c_1(t)e^{-i\int_0^t \Delta\epsilon(t)dt}|u_1(A,t)\rangle$, with $|u_0(A,t)\rangle$ and $|u_1(A,t)\rangle$ the instantaneous driving-amplitude-dependent quasienergy states. The initial values of the coefficients c_0 and c_1 are determined by the representation of the initial qubit state, which is the ground

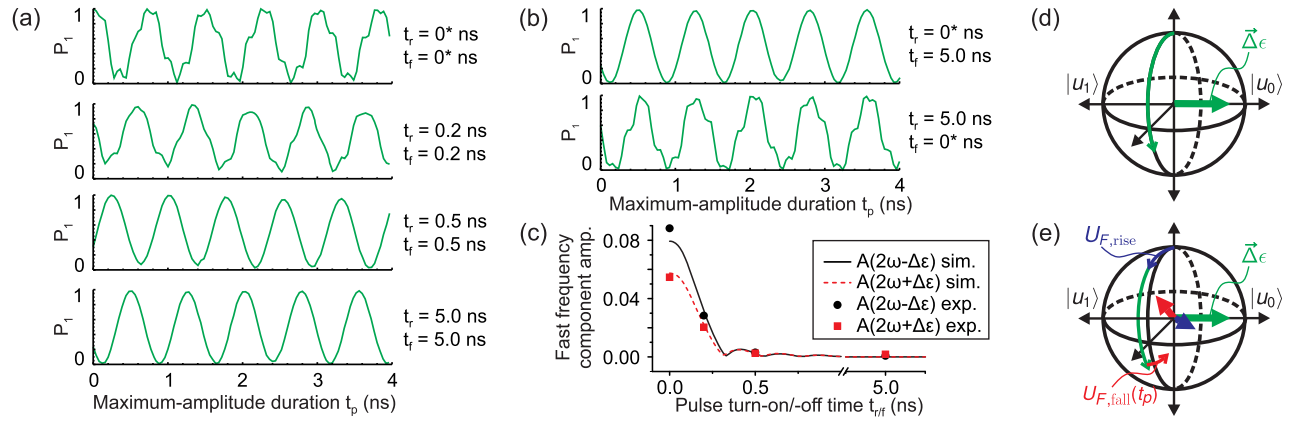

FIG. 4 (color online). (a),(b) Qubit excited state probability P_1 versus pulse duration t_p for various rise (fall) times t_r (t_f) and equal maximum amplitude $A_m = 2\pi \times 1.33$ GHz. Panels (a) and (b) show data with symmetric or asymmetric rise and fall. (c) The measured (dots and squares) and simulated (continuous and dashed lines) fast oscillation amplitudes, at frequencies $2\omega - \Delta\epsilon$ and $2\omega + \Delta\epsilon$, respectively. (d) Adiabatic and (e) nonadiabatic evolution in the Floquet picture. The state is represented on the Bloch sphere, with a basis chosen such that the instantaneous quasienergy states $|u_{0,1}\rangle$ are in the equatorial plane. The state vector evolution (thin arrows) is a rotation around a fictitious field (thick arrows). The initial qubit state is $(|u_0\rangle + |u_1\rangle)/\sqrt{2}$. In the adiabatic case (d), the state evolution is described by a phase $-\int_0^t \Delta\epsilon(t)dt$ applied to $|u_1\rangle$, which is equivalent to rotation around the fictitious field $\vec{\Delta}\epsilon(t)$ aligned with $|u_0\rangle$. In this picture, the evolution of the qubit is a simple rotation, although in the energy eigenbasis the qubit undergoes complex dynamics. In the nonadiabatic case (e), transitions between Floquet states arise during pulse turn-on and turn-off, characterized by the unitary transformations $U_{F,\mathrm{rise}}$ and $U_{F,\mathrm{fall}}$, respectively, which correspond, in general, to rotations around axes that are not parallel to $\vec{\Delta}\epsilon(t)$. The asterisk (*) indicates that the actual rise or fall time is around 20 ps, determined by the analog bandwidth of the AWG.

state, in the basis formed by the states $|u_{0,1}(0,0)\rangle = (|0\rangle \pm |1\rangle)/\sqrt{2}$, with $|0\rangle$ or $|1\rangle$ the ground or excited state of the qubit [31]. For slowly varying driving amplitude $A(t)$, the evolution is adiabatic in the Floquet basis, and therefore the coefficients c_0 and c_1 maintain their initial values. The dynamics of the qubit in this case, using the Bloch sphere representation [see Fig. 4(d)], can be understood by the rotation of the pseudospin representing the state around a fictitious field determined at any given time by the difference $\Delta\epsilon$ between the quasienergies. Similarly to the weak-driving case, the qubit simply undergoes a Rabi rotation between the ground and excited states, with a rotation angle given by $1/2\int_0^t \Delta\epsilon(t)dt$.

With short rise and fall times, the evolution of the qubit at the beginning and end of the pulse is nonadiabatic in the Floquet representation. Nonadiabatic effects can be described by unitary transformations $U_{F,\mathrm{rise}}$ and $U_{F,\mathrm{fall}}$ at the beginning and the end of the pulse, respectively [see Fig. 4(e)]. The latter depends periodically on the pulse duration with period T, leading to fast oscillations of the final state of the qubit. For a driving amplitude $A_m = 2\pi \times 1.33$ GHz, the qubit population dynamics is well described by a sum of oscillatory terms at frequencies $\Delta\epsilon$, $2\omega + \Delta\epsilon$, and $2\omega - \Delta\epsilon$. In Fig. 4(c) we plot the amplitude of the high-frequency components, at $2\omega \pm \Delta\epsilon$, versus the pulse rise and fall time. The experimental results are in good agreement with values extracted based on numerical simulations of the qubit evolution.

In additional experiments [see Fig. 4(b)], we observed the evolution of the qubit with strong pulses and asymmetric rise and fall times. The final state of the qubit displays fast oscillations for pulses with slow rise and fast fall, whereas fast oscillations are absent for pulses with fast rise and slow fall. This observation confirms the asymmetric role of the two rotations, $U_{F,\mathrm{rise}}$ and $U_{F,\mathrm{fall}}$.

We next discuss the use of strong driving for fast quantum gates, specifically qubit state preparation. Starting with the qubit in its ground state, we apply pulses with a driving strength $A_m = 2\pi \times 0.46$ GHz and rise and fall times of approximately 20 ps, defined by the AWG bandwidth. The state $(|0\rangle - i|1\rangle)/\sqrt{2}$ is prepared in 0.48 ns with a fidelity of 0.9996 ± 0.0006 [31]. Similarly, state $|1\rangle$ is prepared in 1.08 ns with a fidelity of 0.9969 ± 0.0008. We have performed numerical simulations of state evolution, which predict state preparation fidelities of 0.9997 and 0.9976 for states $(|0\rangle - i|1\rangle)/\sqrt{2}$ and $|1\rangle$, respectively, in good agreement with the experimental results. Future work should address the optimization of gate fidelities based on randomized benchmarking [4,39,40].

Our work demonstrates the feasibility of using strong driving for the control of superconducting artificial atoms. The dynamics was analyzed in the framework of Floquet theory. The consideration of adiabaticity in the Floquet picture provides a valuable viewpoint on dynamics, applicable well beyond the regime where the rotating wave approximation holds. Our experimental demonstration brings very exciting prospects for experiments addressing the interplay between Floquet dynamics and environmental

effects [41,42]. We expect that our results will stimulate new work across a broad range of fields, including quantum computing, open system dynamics, quantum simulation, and quantum sensing.

We thank Martin Otto, Ali Yurtalan, and Feyruz Kitapli for help with the experiments and the members of the University of Waterloo Quantum Nanofab team for assistance on device fabrication. We would like to thank Kevin Resch and Sergey Shevchenko for comments on the manuscript. We are very grateful to Mark Skadorwa from Tektronix for valuable discussions of technical specifications and facilitating the lending of the AWG used in the experiments. We acknowledge support from NSERC, Canada Foundation for Innovation, Ontario Ministry of Research and Innovation, Industry Canada, and the Canadian Microelectronics Corporation. During this work, C. D. was supported by an Ontario Graduate Scholarship and A. L. was supported by an Early Research Award.

*cdeng@uwaterloo.ca

[1] L. M. K. Vandersypen and I. L. Chuang, Rev. Mod. Phys. **76**, 1037 (2005).
[2] F. Bloch and A. Siegert, Phys. Rev. **57**, 522 (1940).
[3] J. H. Shirley, Phys. Rev. **138**, B979 (1965).
[4] S. Gustavsson, O. Zwier, J. Bylander, F. Yan, F. Yoshihara, Y. Nakamura, T. P. Orlando, and W. D. Oliver, Phys. Rev. Lett. **110**, 040502 (2013).
[5] F. Yoshihara, Y. Nakamura, F. Yan, S. Gustavsson, J. Bylander, W. D. Oliver, and J.-S. Tsai, Phys. Rev. B **89**, 020503 (2014).
[6] W. M. Griffith, M. W. Noel, and T. F. Gallagher, Phys. Rev. A **57**, 3698 (1998).
[7] N. Goldman and J. Dalibard, Phys. Rev. X **4**, 031027 (2014).
[8] M. H. Devoret and R. J. Schoelkopf, Science **339**, 1169 (2013).
[9] J. Q. You and F. Nori, Nature (London) **474**, 589 (2011).
[10] G. G. Paulus, F. Lindner, H. Walther, A. Baltuška, E. Goulielmakis, M. Lezius, and F. Krausz, Phys. Rev. Lett. **91**, 253004 (2003).
[11] G. D. Fuchs, V. V. Dobrovitski, D. M. Toyli, F. J. Heremans, and D. D. Awschalom, Science **326**, 1520 (2009).
[12] S. Saito, M. Thorwart, H. Tanaka, M. Ueda, H. Nakano, K. Semba, and H. Takayanagi, Phys. Rev. Lett. **93**, 037001 (2004).
[13] W. D. Oliver, Y. Yu, J. C. Lee, K. K. Berggren, L. S. Levitov, and T. P. Orlando, Science **310**, 1653 (2005).
[14] M. Sillanpää, T. Lehtinen, A. Paila, Y. Makhlin, and P. Hakonen, Phys. Rev. Lett. **96**, 187002 (2006).
[15] C. M. Wilson, T. Duty, F. Persson, M. Sandberg, G. Johansson, and P. Delsing, Phys. Rev. Lett. **98**, 257003 (2007).
[16] A. Izmalkov, S. H. W. van der Ploeg, S. N. Shevchenko, M. Grajcar, E. Il'ichev, U. Hübner, A. N. Omelyanchouk, and H.-G. Meyer, Phys. Rev. Lett. **101**, 017003 (2008).
[17] G. Sun, X. Wen, Y. Wang, S. Cong, J. Chen, L. Kang, W. Xu, Y. Yu, S. Han, and P. Wu, Appl. Phys. Lett. **94**, 102502 (2009).
[18] J. Tuorila, M. Silveri, M. Sillanpää, E. Thuneberg, Y. Makhlin, and P. Hakonen, Phys. Rev. Lett. **105**, 257003 (2010).
[19] M. P. Silveri, K. S. Kumar, J. Tuorila, J. Li, A. Vepsäläinen, E. V. Thuneberg, and G. S. Paraoanu, New J. Phys. **17**, 043058 (2015).
[20] A. Shytov, D. Ivanov, and M. Feigelman, Eur. Phys. J. B **36**, 263 (2003).
[21] S. Ashhab, J. R. Johansson, A. M. Zagoskin, and F. Nori, Phys. Rev. A **75**, 063414 (2007).
[22] S. Shevchenko, S. Ashhab, and F. Nori, Phys. Rep. **492**, 1 (2010).
[23] Y. Nakamura, Y. A. Pashkin, and J. S. Tsai, Phys. Rev. Lett. **87**, 246601 (2001).
[24] I. Chiorescu, P. Bertet, K. Semba, Y. Nakamura, C. J. P. M. Harmans, and J. E. Mooij, Nature (London) **431**, 159 (2004).
[25] S. Saito, T. Meno, M. Ueda, H. Tanaka, K. Semba, and H. Takayanagi, Phys. Rev. Lett. **96**, 107001 (2006).
[26] K. Drese and M. Holthaus, Eur. Phys. J. D **5**, 119 (1999).
[27] J. E. Mooij, T. P. Orlando, L. Levitov, L. Tian, C. H. van der Wal, and S. Lloyd, Science **285**, 1036 (1999).
[28] T. Niemczyk, F. Deppe, H. Huebl, E. P. Menzel, F. Hocke, M. J. Schwarz, J. J. Garcia-Ripoll, D. Zueco, T. Hummer, E. Solano, A. Marx, and R. Gross, Nat. Phys. **6**, 772 (2010).
[29] P. Forn-Diaz, J. Lisenfeld, D. Marcos, J. J. Garcia-Ripoll, E. Solano, C. J. P. M. Harmans, and J. E. Mooij, Phys. Rev. Lett. **105**, 237001 (2010).
[30] A. Wallraff, D. I. Schuster, A. Blais, L. Frunzio, J. Majer, M. H. Devoret, S. M. Girvin, and R. J. Schoelkopf, Phys. Rev. Lett. **95**, 060501 (2005).
[31] See Supplemental Material at http://link.aps.org/supplemental/10.1103/PhysRevLett.115.133601, which includes Refs. 32–35, for various experimental details and a derivation of analytical expressions for the quasienergies and quasienergy states.
[32] A. A. Abdumalikov, O. Astafiev, Y. Nakamura, Y. A. Pashkin, and J. S. Tsai, Phys. Rev. B **78**, 180502 (2008).
[33] M. Bal, C. Deng, J.-L. Orgiazzi, F. Ong, and A. Lupascu, Nat. Commun. **3**, 1324 (2012).
[34] B. Efron and R. Tibshirani, *An Introduction to the Bootstrap*, in Monographs on Statistics & Applied Probability (Chapman and Hall/CRC, Boca Raton, 1994).
[35] S.-K. Son, S. Han, and Shih-I. Chu, Phys. Rev. A **79**, 032301 (2009).
[36] J.-L. Orgiazzi, C. Deng, D. Layden, R. Marchildon, F. Kitapli, F. Shen, M. Bal, F. R. Ong, and A. Lupascu, arXiv:1407.1346.
[37] M. Stern, G. Catelani, Y. Kubo, C. Grezes, A. Bienfait, D. Vion, D. Esteve, and P. Bertet, Phys. Rev. Lett. **113**, 123601 (2014).
[38] C. E. Creffield, Phys. Rev. B **67**, 165301 (2003).
[39] R. Barends *et al.*, Nature (London) **508**, 500 (2014).
[40] S. Sheldon, L. S. Bishop, E. Magesan, S. Filipp, J. M. Chow, and J. M. Gambetta, arXiv:1504.06597.
[41] M. Grifoni and P. Hänggi, Phys. Rep. **304**, 229 (1998).
[42] M. Moskalets and M. Büttiker, Phys. Rev. B **66**, 205320 (2002).